12WCEE 2000

INPUT MOTION OF A RIGID EXTENDED FOUNDATION DUE TO SPATIALLY VARIABLE SEISMIC GROUND MOTION

Hirotoshi UEBAYASHI[1] And Yoshihiro TAKEUCHI[2]

SUMMARY

The dynamic behavior of an actual embedded foundation caused by spatial variation of seismic ground motion is evaluated through the comparison between actual measurement and theoretical calculation. The foundation input motion in the actual measurement was assumed from the foundation response caused by earthquakes and the dynamic ground compliance functions obtained by excitation experiment, while the theoretical foundation input motion was calculated based on the spatial-correlation model of seismic motions assumed from the horizontal array observation at the free-field around the foundation. The foundation input motions are simulated by the spatial weighted averages of free-field ground motions which are presented, typically, as linear functions of position of foundation. Spatially incoherent seismic ground motions are generated using the relation between the coherency function and statistical properties of the Fourier phase angle. We obtained mainly the following conclusions: As for horizontal-translational and torsional components of the foundation input motion, theoretical results calculated from the realistic spatial-correlation model of seismic ground motions that is suited to the proposed site, almost agreed with the average value of the actual measurement for thirteen events.

INTRODUCTION

In recent papers, spatial variation of seismic ground motion has been presented quantitatively through the analysis of seismic ground motions recorded by high-dense array experiments. According to these papers, spatial variation of seismic ground motion induced by a spatially-incoherent component, in general, has been modeled as a function of frequency and separation distance(e.g. Abrahamson,1991, Harichandran,1986). Moreover, since spatial variation of seismic ground motion includes time shift caused by the wave-passage effect(Vanmarcke,1992), it cannot be ignored in designing a rational earthquake-resistant design of the structure on foundation ranging from dozens of meters to several hundreds of meters. Spatial variation of seismic ground motion causes decrease in the translational response of foundation; on the other hand, it induces the torsional and rocking responses of foundation. The effect of spatial variation of seismic ground motion on the foundation input motion has been theoretically proved by Loco (1986), Yoshida (1988), and other researchers, through their study on an ideal spatial-correlation model of seismic motions. However, in order that spatial variation of seismic ground motion including randomness may be reflected in earthquake-resistant design, it is necessary to evaluate the relationship between the spatial-correlation of seismic ground motion and the dynamic behavior of an actual foundation, based on the measurement at an actual site.

In this study, the dynamic behavior of an actual embedded foundation caused by spatial variation of seismic ground motion is evaluated through the comparison between actual measurement and theoretical calculation. The foundation input motion in the actual measurement was assumed from the foundation response caused by earthquakes and the dynamic ground compliance functions obtained by excitation experiments, while the theoretical foundation input motion was calculated based on the spatial-correlation model of seismic motions assumed from the horizontal array observation at the free-field around the foundation.

[1] *Dept. of Architecture, Junior college, Osaka Inst of Tech., Omiya 5-16-1 Osaka 535-0002, Japan, ueba@archi.oit.ac.jp*
[2] *Dept. of Architecture, Osaka Institute of Tech., Omiya 5-16-1 Osaka 535-0002, Japan, takeuchi@archi.oit.ac.jp*

ARRAY OBSERVATION AND GEOLOGICAL CONDITION

The object site is located in a littoral region of Tadotsu-cho in Kagawa Prefecture facing the Inland Sea of the Western Japan. As for its geological condition, alluvial layered medium consisting of clay lies on the surface, below which diluvial layered medium mainly consisting of sand and gravel is accumulated to the depth of GL-160 meters. Below GL-160 meters, granite bedrock can be found. Table 1 shows an assumed subsurface structure. Array observations on the foundation and in its surroundings were conducted from 1980 to 1986. Fig. 1 shows the reinforced-concrete mat foundation and the location of observation points. As for a component of an accelerometer at each observation point, the points P2, P3, and P4 on the foundation have one component X, Y, and Z, respectively; and the other points have three components. Table 2 shows the information of the events used in the analysis. The epicentral direction of these events is slightly inclined to the direction of the long side (X) from the center of the foundation.

Table 1 Geophysical constants of multi-layered strata

Layer	Thickness	S-wave velocity	Density	Q-value
1	10 (m)	150(m/s)	1.85(t/m3)	10
2	39	330	2.00	25
3	31	410	2.00	30
4	34	515	2.10	30
5	22	650	2.10	30
6	25	900	2.20	30
7	——	1700	2.50	60

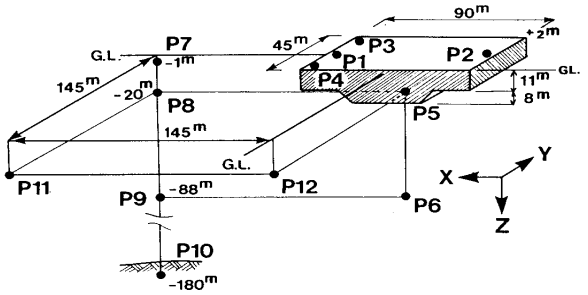

Fig.1 Configuration of the array observation

CORRECTION OF ORIENTATION ERROR OF SEISMOMETER

As seismicity in the Western Japan was low during the observation period, the observed maximum accelerations were small as shown in Table 2. The S/N ratio of recorded accelerographs was examined using band-pass filtered waves, the result of which was favorable (=S/N ratio was high) in the range of 0.3 to 18.0 Hz. In this study, the main S-wave portion with the duration of 4.5 to 8 seconds was used in the analysis. In order to examine the orientation error of embedded seismometers, coherence analysis was conducted on the measurement results between a point on the foundation (P1) and embedded points (P5 to P12). The orientation error was estimated by regarding a band-pass filtered waveform (0.3 to 2.0 Hz) with two horizontal components as vector time series, and finding out a coordinate rotation angle on Z-axis with the maximum coherence to X component on the reference point P1. The estimated error angles are shown in Table 3. Fig. 2 shows the waveforms before and after the correction of orientation errors for EQ 5. The waveforms of the main S-wave portion at each observation point after the correction agree better with each other than before the correction.

Event	Date(m.d.yr)	MJMA	Lat.N	Long.W	Depth(km)	Epic.dist.(km)	Max.Acc.(gal)
1	04/25/84	4.2	34•41'	133•33'	22	52	2.9
2	05/30/84	5.6	34•58'	134•36'	17	108	12.9
3	05/30/84	5.0	34•55'	134•37'	16	108	7.5
4	06/02/84	4.3	34•58'	134•35'	18	107	3.5
5	06/25/84	5.2	34•45'	132•35'	12	121	15.9
6	04/17/85	4.2	33•29'	133•12'	39	111	6.3
7	09/27/85	4.7	33•42'	134•45'	47	121	5.9
8	10/22/85	4.6	34•42'	134•43'	13	98	2.2
9	01/06/85	5.7	34•10'	135•33'	70	179	4.3
10	01/27/85	6.0	32•36'	131•17'	118	319	4.5
11	04/05/85	5.3	33•31'	131•34'	118	249	5.5
12	05/13/85	6.0	32•59'	132•35'	39	184	7.3
13	07/02/85	4.9	35•22'	133•36'	14	122	5.1

Table 2 Information of events

Observ. point	P1	P2	P3	P4	P5	P6	P7	P8	P9	P10	P11	P12
Orient. error(degree)	0	0	0		15	-63	-131	-117	59	-130	-125	-125

Table 3 Estimated orientation error angles of seismometers

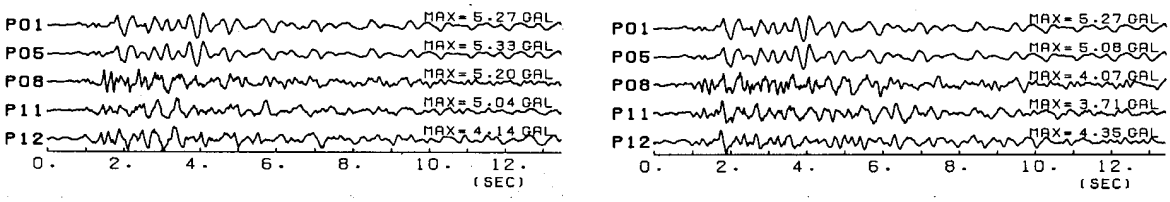

Fig.2 Time histories before (left) and after (right) the correction of orientation errors

FORMULATION OF FOUNDATION INPUT MOTION TAKING INTO ACCOUNT SPATIAL VARIATION OF SEISMIC GROUND MOTION

A foundation input motion vector $\{U^*_o\}$ at the reference point on the foundation can be expressed in the frequency domain as follows (Luco, 1986), using a free-field motion vector $\{U_g(x)\}$ and a free-field traction

$$\{U^*_o\} = [C] \int_S [\overset{\upsilon}{\Gamma}_R(\bar{x})]^T \{U_g(\bar{x})\}\, ds(\bar{x}) - [C] \int_S [\alpha(\bar{x})]^T \{\overset{\upsilon}{T}_g(\bar{x})\}\, ds(\bar{x}) \quad , \bar{x} \in S \tag{1}$$

vector $\{T_g(x)\}$ on the contact surface, *S*, between the foundation and the soil:

Where, $\{U^*_o\} = \{U^*_{oi}\ (i = 1,2...., 6)\}^T$, $\{U_g(x)\} = \{U_{gj}(x))\ (j = 1,2,3)\}^T$, and $\{T_g(x)\} = \{T_{gj}(x)\ (j = 1,2,3)\}^T$. (*i,j = 1,2,3*: the translational components *X,Y,* and *Z*; *4,5,6*: the rotational components around the axes *X,Y,* and *Z*.) [C] is a compliance matrix of 6 x 6, and an inverse matrix of an impedance matrix [K]. $[\Gamma_R(x)]$ is a matrix of 3 x 6 having $\Gamma^{ji}{}_R(x)$ as a component (which is *j* component of free-field traction on *S* when the foundation is given unit displacement only to *i* component). A subscript *R* represents the assumption of rigid foundation. $[\alpha(x)]$ is a matrix of 3 x 6 having $\alpha^{ji}(x)$ as a component (which is a transformation coefficient to transform *j* component traction acting on *S* into *i* component force vector at the reference point on the foundation). When there is no embedded foundation, the second term in Eq. (1) can be neglected. It is quite difficult to obtain the exact solution of $\Gamma^{ji}{}_R(x)$ when the foundation has an arbitrary form embedded in multi-layered subsurface structure. Therefore, assuming that $\Gamma^{ji}{}_R(x)$ becomes approximately linear functions of position on S, it can be replaced as $[\Gamma_R(x)] = [\alpha(x)]\,[H]^{-1}[K]$. The following equation can be obtained:

Compared with the exact solution, a relatively favorable approximation can be obtained by Eq. (2), as shown by Iguchi (1982) based on the torsional response of a cylindrical foundation embedded in a half-space. In order to make it possible to calculate the foundation input motion of an embedded foundation using only free-field

$$\{U^*_o\} = [H]^{-1} \int_S [\alpha(\bar{x})]^T \{U_g(\bar{x})\}\, ds(\bar{x}) - [C] \int_S [\alpha(\bar{x})]^T \{\overset{\upsilon}{T}_g(\bar{x})\}\, ds(\bar{x}) \ , \ \text{where} \ \ [H] = \int_S [\alpha(\bar{x})]^T [\alpha(\bar{x})]\, ds(\bar{x}) \tag{2}$$

motion, Kurimoto et al. (1996) proposed the following equation, using the condition that the resultant force at the reference point on the foundation caused by free-field traction on *S* is equivalent to that caused by inertia force in free-field region:*V* inside *S*:

$$\{U^*_o\} \cong [H]^{-1} \int_S [\alpha(\bar{x})]^T \{U_g(\bar{x})\}\, ds(\bar{x}) - \omega^2 [C] \int_V \rho(\hat{x}) [\alpha(\hat{x})]^T \{U_g(\hat{x})\}\, dV(\hat{x}) \tag{3}$$

$$\begin{Bmatrix} U^*_{ox} \\ \Phi^*_{oy} \end{Bmatrix} = \frac{1}{AI_y - \gamma^2} \begin{pmatrix} I_y & -\gamma \\ -\gamma & A \end{pmatrix} \left\{ \begin{array}{l} \int_S U_{gx}(x)\, ds(\bar{x}) \\ \int_S [\bar{Z}_o U_{gx}(\bar{x}) - \bar{X}_o U_{gz}(x)]\, ds(\bar{x}) \end{array} \right\} - \omega^2 \begin{pmatrix} C_{xx} & C_{x\theta_y} \\ C_{\theta_y x} & C_{\theta_y \theta_y} \end{pmatrix} \left\{ \begin{array}{l} \int_V U_{gx}(\hat{x})\, dV(\hat{x}) \\ \int_V [\hat{Z}_o U_{gx}(\hat{x}) - \hat{X}_o U_{gz}(\hat{x})]\, dV(\hat{x}) \end{array} \right\} \tag{4}$$

$$\Phi^*_{oz} = \frac{1}{I_z} \int_S [-\bar{Y}_o U_{gx}(\bar{x}) + \bar{X}_o U_{gy}(\bar{x})]\, ds(x) - \omega^2 C_{\theta_z \theta_z} \int_V [-\hat{Y}_o U_{gx}(\hat{x}) + \hat{X}_o U_{gy}(\hat{x})]\, dV(\hat{x})$$

$$\text{where} \ \ A = \int_S ds(x) \ , \ \ \gamma = \int_S Z_o\, ds(\bar{x}) \ , \ \ I_y = \int_S [\bar{X}^2_o + \bar{Z}^2_o]\, ds(\bar{x}) \ , \ I_z = \int_S [\bar{X}^2_o + \bar{Y}^2_o]\, ds(\bar{x})$$

From Eq. (3), the equation of the translational response in the *X* component and the rotational response on the Y and *Z* axes can be obtained as follows:

When the reference point on the foundation is given as (x_o, y_o, z_o), $\bar{X}_o = x - x_o$, $\bar{Y}_o = y - y_o$, and $Z_o = z - z_o$, on the surface S; $X_o = x - x_o$, $Y_o = y - y_o$, and $Z_o = z - z_o$ in the volume V. The integral term in Eq.

$$\int_S U_{gx}(\bar{x})\, ds(x) \cong \sum_{m=1}^{M} U_{gx}^m \Delta S_m \ , \quad \int_V U_{gx}(\hat{x})\, dv(\hat{x}) \cong \sum_{n=1}^{N} U_{gx}^n \Delta V_n$$

$$\int_S [\bar{Z}_o U_{gx}(\bar{x}) - \bar{X}_o U_{gz}(\bar{x})]\, ds(\bar{x}) \cong \sum_{m=1}^{M} [(z_m - z_o)U_{gx}^m - (x_m - x_o)U_{gz}^m]\Delta S_m \qquad (5)$$

$$\int_V [\hat{Z}_o U_{gx}(\hat{x}) - \hat{X}_o U_{gz}(\hat{x})]\, dv(x) \cong \sum_{n=1}^{N} [(z_n - z_o)U_{gx}^n - (x_n - x_o)U_{gz}^n]\Delta V_n$$

(4) can be calculated by discrete integration as follows:

Where, M and N are the number of descretized partitions of the surface S and the volume V, respectively. The mth partitioned area element and the nth partitioned volume element are ΔS_m and ΔV_n, respectively. U_{gx}^m and U_{gx}^n represent X components of free-field motion at the representative point (centroidal point) of ΔS_m and ΔV_n, respectively.

It is assumed that the accuracy of solution of the foundation input motions depends on the number of partitions to be discretized. Therefore, the results of exact solution shown by Luco et.al.(1986) and those obtained by the method presented in this study are compared in Fig.3. The lines of three kinds in Fig. 3 shows the translational response in the X component and torsional component of the input motion of the rectangular foundation placed on the ground surface, using the number of partitions as a parameter. The coherence function used in the calculation is shown in the following equation:

$$\mathrm{coh}\ (\ f\ ,\ r\ )\ =\ \exp\{-(\gamma\omega r/\beta)^2\} \qquad \textbf{(6)}$$

Where, $\gamma = 0.15$, $\omega = 2\pi f$, $\beta = 530$ m/s, r = separation distance. As shown in Fig. 3, a good agreement with the exact solution can be seen regardless of the number of partitions if the number of partitions is 4 or more, which implies it is possible to calculate foundation input motion with accuracy using the method of discrete integration. Foundation total motion $\{U_o\}$ corresponding to the foundation input motion can be obtained from the following equation:

$$\{Uo\} = ([I] - \omega^2 [C][M])^{-1} \{Uo^*\} \qquad \textbf{(7)}$$

Where, [I] is a unit matrix, and [M] is a mass matrix of the foundation. In this study, a reference point on the foundation is set on the position of the bottom in the center of foundation (at the same position as P5).

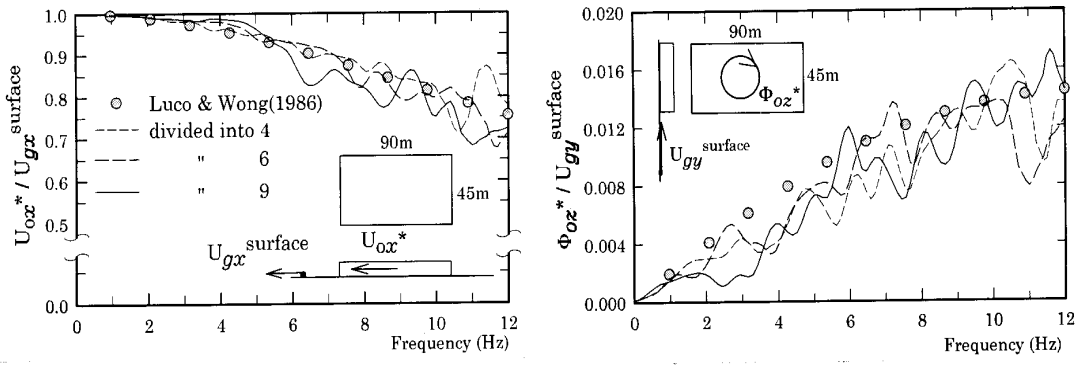

Fig.3 Comparison of the foundation input motion in translational and torsional components between exact solutions shown by Luco et.al.(1986) and the method presented in this study.

Excitation experiments were conducted on the foundation(Tajimi, 1984). A solid line in Fig. 4 shows real, imaginary and absolute value of a complex compliance function in X component, Cxx, obtained from the experiments; a broken line in Fig. 4 shows the compliance function calculated from a list of impedance functions of a square embedded foundation proposed by Mita et al. (1989). Here, the following parameters were used: S-wave velocity as 260 m/s, the poisson's ratio as 0.4, the ratio of the foundation depth to half-width of a square foundation as 0.5, and half-width as 32 m. The solid and broken lines show good agreement in general.

Therefore, the torsion and rocking of a compliance function that are not obtained from the experiments were calculated by the inverse of impedance functions proposed by Mita et.al..

SPATIAL-CORRELATION MODEL OF SEISMIC GROUND MOTION BASED ON OBSERVATION

In order to model the spatial-correlation of seismic ground motion at the Tadotsu site, coherences for three observational points at GL-20 meters was obtained from Eq. (8) as the average of 13 events(Table2):

$$coh_{jk}(f) = |Sj_k(f)| / [S_{jj}(f)\, S_{kk}(f)]^{1/2} \quad \textbf{(8)}$$

Were, S_{jk} is a cross-spectral density function between the points j and k; S_{jj} and S_{kk} are power-spectral density functions at j and k, respectively. These density functions are smoothed by a Bartlett-type window with a band width of 0.4 Hz. Fig. 5 shows coherences for P8 and P11, and P11 and P12 where separation is 145 meters. The standard deviation of the coherences is also shown in Fig. 5. The symbol ○ is a coherence model observed at Lotung LSST array as shown in Eq. (9)(Abrahamson, 1991); □ is a coherence model obtained from Eq. (6) using $\gamma = 0.3$ and $\beta = 530$ m/s. Coherences at Tadotsu site agrees well with the LSST model, though the data on source parameters, and wave-path differ. This is considered to be the result of similarity between Tadotsu site and LSST site in the velocity structure of surface geology(see Abrahamson,1991). Moreover, Schneider (1994) pointed out that LSST model agrees well with the spatial correlation at other sedimentary sites.

$$\tanh^{-1}|coh(f,r)| = (2.54 - 0.012\, r)[\exp\{(-0.115 - 0.00084\, r)f\} + 0.33f^{-0.878}] + 0.35 \quad \textbf{(9)}$$

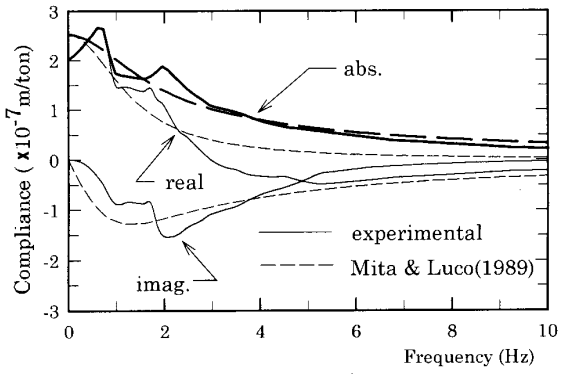

Fig.4 Comparison of compliance functions of X-comp between theoretical result shown by Mita et.al. (1989)

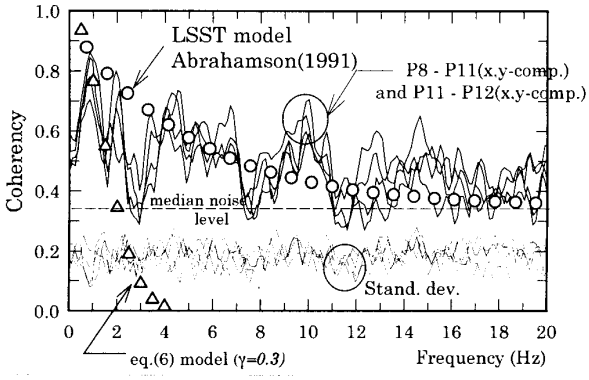

Fig.5 Comparison of coherences for separation distance 145m between the few models and estimations

GENERATION OF SPATIALLY-INCOHERENT SEISMIC MOTION

Fig. 6 shows a foundation plan and a cross section of the foundation-ground system. The representative points of the area element and the volume element, which are input points of free-field motion as mentioned above, are expressed by a symbol ● (m = 1, 2, ...20) and a symbol ○ (n = 1,2,...18), respectively. The depth of each representative point is shown by A, B, C, D, and E, and a reference level (GL –20 meters) is shown by R. Free-field seismic motion at a representative point was generated according to the following three steps:

(1) A stationary random reference motion was generated at the point □ on the reference level shown in Fig. 6. As a Fourier amplitude characteristic, this reference motion has a band-limited white noise with 10 gal*sec within the frequency range between 0.2 to 13.0 Hz; and as a phase characteristic, it has a uniform random number distributed between $-\pi$ and π.

(2) Based on this reference motion, a set of spatially-incoherent seismic motions in accordance with Eq. (9) was generated for 12 points just under the symbol □ on the reference level, using the method proposed by Abrahamson (1992). Fig. 7 shows an example of a set of generated waveforms. In order to verify the accuracy of these waveforms, coherences was obtained for the couples of waveforms with several

separations, as shown in Fig. 8. Coherences obtained from a sample of the waveforms agrees well with a target coherence function. The wave-passage effect can be evaluated by giving time shift to a set of the waveforms obtained. In this study, time shift corresponding to apparent phase velocity 3 km/s is given to the direction of the long side of the foundation.

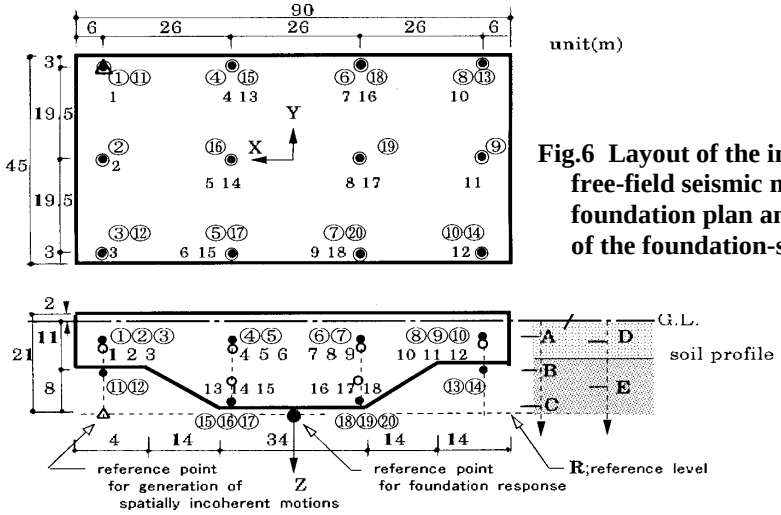

Fig.6 Layout of the input points of free-field seismic motions, a foundation plan and a cross section of the foundation-soil system.

(3) Seismic ground motions at a total of 38 representative points (shown by symbols ● and □) were generated by multiplying a Fourier spectrum of seismic ground motions generated at 12 points on the reference level by a transfer function based on the one-dimensional multi-layered reflection theory. Fig. 9 shows transfer functions at five levels of input points (A to E) to the reference level R. In order to verify the validity of these transfer functions, the transfer functions at P7 to P8 obtained by the measurement were compared with the theoretical transfer functions in Fig. 10. Theoretical transfer functions almost agree with the measured values in the wide frequency range. Based on a set of seismic ground motions of the 38 components generated, the foundation input motion can be calculated using Eq. (4).

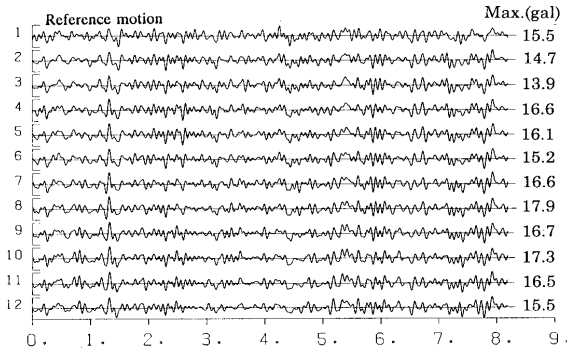

Fig.7 Generated spatially-incoherent time histories at a depth of 21m just under the twelve points shown

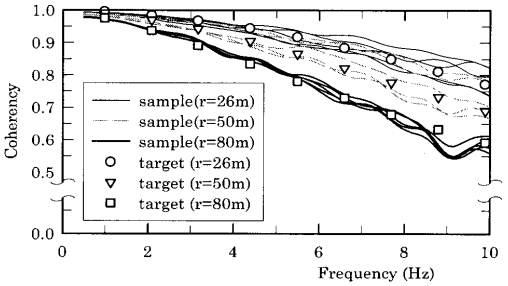

Fig.8 Comparison of coherences obtained for the couples of the generated time histories(Fig.7)

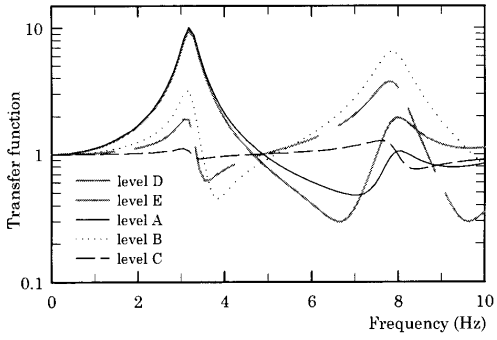

Fig.9 Transfer functions at five levels(A to E) to the reference level:R(-21m) (see Fig.6).

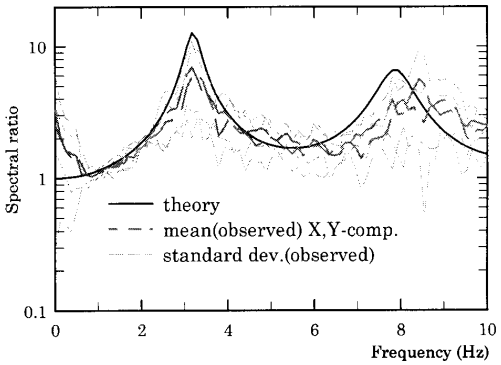

Fig.10 Comparison of transfer functions between theory and measurements(P7 to P8)

COMPARISON OF FOUNDATION INPUT MOTIONS OBTAINED FROM THEORY AND ACTUAL MEASUREMENT

In Fig. 11, the foundation input motions of *X* translational component U^*_{ox} calculated theoretically is compared with the one obtained from the actual measurement. These foundation input motions were normalized by free-surface motion $U_{gx}^{surface}$. As foundation input motion cannot be measured directly, *X* translational component in Eq. (7) is replaced with the following Eq. (10); then by replacing the foundation total motion U_{ox} in the right term with the observed seismic motion at P5, it was evaluated

$$U^*_{ox} / U_{gx}^{surface} = (1 - m\omega^2 Cxx)\, U_{ox} / U_{gx}^{surface} \qquad \textbf{(10)}$$

Free-surface motion $U_{gx}^{surface}$ was obtained by multiplying Fourier spectrum at the observation points P11 and P12 on the reference level by the theoretical transfer function shown in Fig. 10. Foundation input motions for actual measurements for P11 and P12 are shown in Fig. 11. The symbols ● and □ show the average of 13 events, and error bars show standard deviations. Three curves show the foundation input motions obtained from the theoretical calculation. Among these curves, a thick solid line shows the result when both a spatially-incoherent component (a coherence model in Eq. (9)) and time shift due to the wave-passage effect (3 km/s) are taken into consideration at the same time. A thin solid line shows the result when S-wave with a uniform waveform is vertically incidence. A broken line shows the result when only an incoherent component [γ = 0.3, β = 530 m/s] of a coherence model in Eq. (6) is taken into consideration. In the theoretical calculation, a thick solid line shows about 10% smaller values than a thin solid line at 5Hz and about 20% smaller at 8Hz. The thick solid line agrees well with the average of actual measurements. A broken line shows too small foundation input motion compared with the actual measurement. These results imply that when obtaining the foundation response in consideration for spatial variation of seismic ground motions, it is necessary to provide a realistic spatial-correlation model of seismic motions that is suited to the object site.

Fig. 12 shows the comparison between a translational component of foundation total motion calculated from the theoretical foundation input motion shown by a thick solid line in Fig.11 and a measured translational response(seismic motions recorded at P5). It is obvious from the figure that both responses agree well. According to the comparison of thick lines in Fig. 11 and Fig. 12, a drop in response due to inertial interaction is 40% at 5Hz, and 50% at 8Hz.

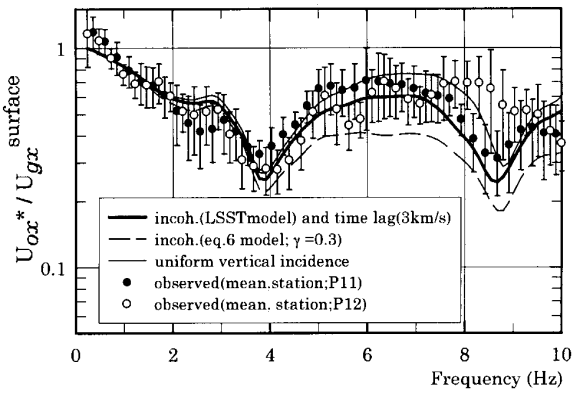

Fig.11 Comparison of the foundation input motion of X translational component between the simulations

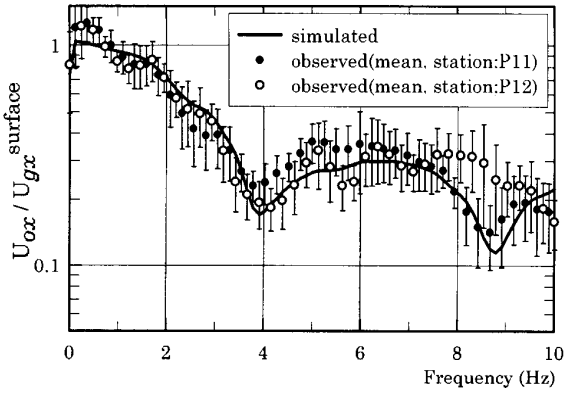

Fig.12 The same as Fig.11, but for the foundation total motion

Fig. 13 shows the response of a normalized torsional component corresponding to a translational component shown in Fig. 12. A torsional component of actual measurements is evaluated using the following equation:

$$\Phi_{oz} = (P1y - P5y)/Dx - (P4z - P1z)/Dy \square (Dz/Dx) \qquad \textbf{(11)}$$

Were, P1y, for example, shows *Y* component of a seismic motion at the observation point P1. *Dx*, *Dy*, and *Dz* are the distance from the reference point (P5) to the end of the long side(44m), to the end of the short side(22m), and to the upper end (21m) of the foundation, respectively. By applying Fourier transformation to Eq. (11), the frequency response can be obtained. The foundation response obtained by the theoretical calculation stayed within the range of standard deviations of actual measurements, showing agreement with the actual measurement

in terms of the tendency to increase in the frequency domain of 1Hz or more. This result shows that torsional response was induced by spatial variation of seismic ground motions.

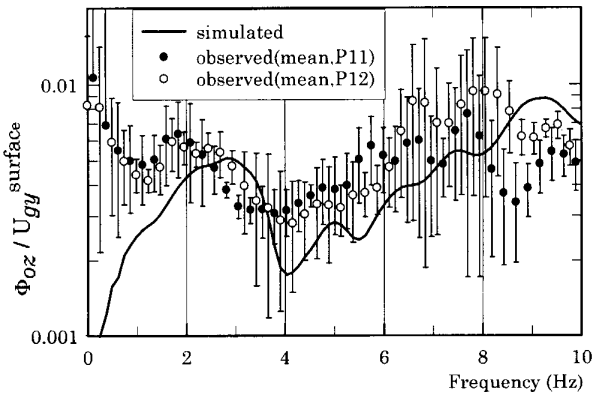

Fig.13 Comparison of the foundation total motion of torsional component between the simulation and the actual measurements

CONCLUSIONS

We obtained the following four conclusions:

1) As for a horizontal translational component of foundation input motions, theoretical results calculated from the realistic spatial-correlation model of seismic motions that is suited to the proposed site, almost agreed with the average value of the actual measurement. Input loss due to spatial variation of seismic ground motions and wave-passage effect was about 20% at 8Hz.

2) As for a torsional component, the foundation total response obtained from the theoretical calculation showed the tendency that response increases in proportion with an increase in frequency, which agrees well with the actual measurement.

3) When obtaining foundation input motions of an embedded foundation, the embedded effect such as variation of the amplitude characteristics of free-field motions in vertical direction can be evaluated by a transfer function of one-dimensional multi-layered reflection theory.

4) LSST model (Abrahamson, 1991), which is a spatial-correlation model of seismic motions used in this study, can be used as a input motion model for the foundation of structure (with a scale within 100 meters) built on the sedimentary site.

REFERENCES

Abrahamson,N.A., Schneider,J.F. and Stepp,J.C. : Empirical spatial coherency functions for application to soil-structure interaction analyses, "*Earthquake Spectra,*" Vol.7, pp.1-27, 1991.1

Abrahamson,N.A. :Generation of spatially incoherent strong motion time histories, *"Proc. 10th W.C.E.E."*, Vo.2, pp.845-850, 1992.

Harichandran,R.S. and Vanmarcke,E.H. : Stochastic variation of earthquake ground motion in space and time, "*J. Eng. Mec. ASCE"*,Vol.112, pp.154-174,1986

Iguchi, M. : An approximate analysis of input motions for rigid embedded foundations, *"Trans. A.I.J."*, Vol.315,pp.61-73,1982.5.

Kurimoto,O. and Iguchi,M.:Evaluation of foundation input motions based on observed seismic motions, "*11th W.C.E.E.*, No317, 1994.

Luco,J.E. : Response of a rigid foundation to a spatially random ground motion, *"E.E.S.D."*,, pp.891-908, 1986.

Luco,J.E. : On the relation between radiation and scattering problems for foundations embedded in an elastic half-space, *"S.D.E.E."*, Vol.5,pp.97-101,1986.

Mita,A. and Luco,J.E. : Impedance functions and input motions for embedded square foundations, "*J. Geotech. Eng., ASCE"*, Vol.115, pp.491-503, 1989.4.

Tajimi,H. :Predicted and measured vibrational characteristics of a large-scale shaking table foundation, *"Proc 8th W.C.E.E.,"* pp.873-880,1984.

Vanmarcke,E.H. : Local spatial variation of earthquake ground motion, *"Proc. W.C.E.E."*, pp.6615-6620, 1992.

Yoshida,K. and Mita,A. : Dynamic response of embedded foundations to a spatially random ground motion, *"Proc. 9th W.C.E.E."*, Vol.3, pp.361-366,1988.